Acta Materialia 124 (2017) 446–455

Contents lists available at ScienceDirect

Acta Materialia

journal homepage: www.elsevier.com/locate/actamat

Full length article

# Blistering in semi-solid die casting of aluminium alloys and its avoidance

X.G. Hu [a, b, c], Q. Zhu [a, d, *], S.P. Midson [a, e], H.V. Atkinson [c], H.B. Dong [c], F. Zhang [a], Y.L. Kang [b]

[a] General Research Institute for Nonferrous Metals, 100088, Beijing, China
[b] University of Science and Technology Beijing, 100083, Beijing, China
[c] Department of Engineering, University of Leicester, LE1 7RH, UK
[d] Southern University of Science and Technology, 518055, Shenzhen, China
[e] Colorado School of Mines, Golden, CO, 80401, USA

ARTICLE INFO

*Article history:*
Received 25 July 2016
Received in revised form
10 November 2016
Accepted 11 November 2016
Available online 18 November 2016

*Keywords:*
Blistering
Semi-solid die casting
Process window
Heat treatment
Aluminium alloy 319s

ABSTRACT

Semi-solid die casting of relatively high solid-fraction aluminum alloys (0.5–0.7 fraction solid) can be used for the production of high quality industrial components. However, surface blistering during solution heat treatment can still be a problem and is associated with the entrapment of gas whether from air or from burned lubricant. Here the mechanism for formation of blisters is presented. The Reynolds number *in the surface layer* of the semi-solid flow is then analysed to obtain the relationships with hydraulic diameter and flow velocity for different slurry temperatures. The hypothesis is that it is some flow instability at the flow front, even where the overall nature of the flow is essentially laminar, which is leading to the entrapment. The crucial finding is that if the Reynolds number is plotted against temperature there is a decrease followed by an increase. The position of this minimum is dependent on the ratio of fill velocity to the hydraulic diameter, *v/D*. Thus there is a 'sweet spot' in terms of temperature (*i.e.* fraction liquid), flow velocity and hydraulic diameter (*i.e.* die design) where the flow front has the maximum stability, giving maximum resistance to blister formation. This is in contrast with conventional wisdom which would suggest that low fractions liquid would give the most stable flow front. A rationale for this is presented in terms of the particle crowding at the relatively low fraction of liquid.

Experimental results with aluminium alloy 319s as an exemplar, and a die which has varying cross sectional dimensions, are presented and validate the hypothesis.



## 1. Introduction

Components produced by conventional high pressure die casting (HPDC) are typically not heat treated due to the presence of casting defects such as entrapped air and lubricants that cause surface blistering during solution heat treatment [1]. The gases and lubricants are entrapped beneath the surface of the castings due to the non-planar and turbulent flow conditions during cavity filling, as illustrated by Fig. 1a. Several high integrity die casting processes, *e.g.* high-vacuum die casting, squeeze casting and semi-solid die casting, have been developed to overcome this entrapment problem [2].

Semi-solid die casting is a semi-solid processing (SSP) technique that is gaining increasing industrial application, especially in Asia with light alloys such as aluminium and magnesium [3]. Unlike other casting processes, it does not utilize a fully liquid feed material, but instead uses a material that is partially solid and partially liquid (as reviewed in Ref. [4]). The slurry is injected into a reusable steel die, and once the cavity is fully filled, an intensification pressure is applied as the slurry solidifies, to feed solidification shrinkage. The flow regimes for semi-solid alloys with relatively low solid fractions have been characterized by Janudom et al. [5] based on the ratio of gate speed to initial solid fraction ($v_g/f_s$). With higher solid fractions ($0.5<f_s<0.7$) the high viscosity feed material exhibits laminar flow with a smooth flow front if the process parameters are carefully controlled (Fig. 1b). Therefore, semi-solid die castings typically contain significantly lower levels of

* Corresponding author. Department of Mechanical and Energy Engineering, Southern University of Science and Technology, 518055, China.
*E-mail address:* zhuq@sustc.edu.cn (Q. Zhu).

http://dx.doi.org/10.1016/j.actamat.2016.11.032

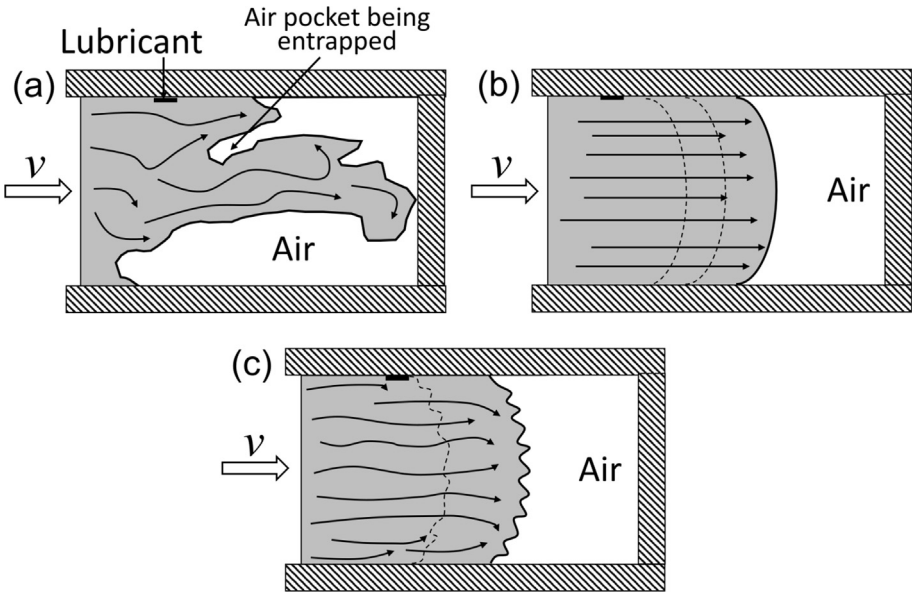


**Fig. 1.** Graphic illustrations showing different types of flow (a) Non-planar and turbulent flow in conventional high pressure die casting, (b) Planar and laminar flow with high stability in semi-solid processing and (c) Planar and laminar flow with some instability at the semi-solid/gas interface.

entrapped gases and lubricants when compared with conventional HPDC components, allowing them to be heat treated to optimize mechanical properties.

In practice, however, blistering can still be an issue for the commercial production of semi-solid die castings when the process has not been fully optimised [6]. Fig. 1c illustrates the semi-solid flow where there is less flow front stability compared with the flow in Fig. 1b. As a result, some air and lubricants are likely to be entrapped, especially at the locations near the wall. To avoid blistering, commercial aluminium semi-solid castings are often processed using only artificial aging procedures, *i.e.* T5 heat treatment [7], rather than the full solution plus aging treatment, *i.e.* T6 heat treatment [8]. By settling for the T5 procedure, however, one of the major advantages of semi-solid casting processes, namely the ability to generate significantly improved mechanical properties, is not realized. Therefore, it is highly desirable to understand the mechanisms in semi-solid castings, to minimize (or eliminate) blistering during the commercial production of semi-solid castings, thereby broadening the commercial appeal of these types of castings. It should be emphasised that surface blisters occur because of the expansion of gases at high temperature during the solution heat treatment. This process is thought to be the same in both semi-solid and conventional die casting processes, but it is the mechanism of gas entrapment during the die filling process which is significantly different. The level of blistering is determined by the volume and location of the entrapment.

In the present study, the nature of blistering will be examined, the mechanisms of blistering formation during heat treatment will be theoretically analysed, and then factors affecting formation of the blistering will be discussed in term of a 'modified' "Reynolds Number". (The term 'modified' is used here to emphasise that it is the shear rate dependent viscosity which has been used in the formula rather than a constant one). Experimental validation of this theoretical analyses will also be presented, using aluminium alloy 319s as an exemplar. It should be noted that semi-solid die casting practice should ensure that hydrogen contamination is avoided and so it is the entrapment of air/lubricants which is the focus here. The core aim of the paper is assisting with the avoidance of blistering in commercial practice through improved understanding of the control of process parameters.

## 2. Mechanism of blistering formation

### 2.1. Nature of blistering in semi-solid die casting

Fig. 2 shows the typical morphology of blisters in a semi-solid casting of 319s alloy. The metal close to the casting surface is plastically deformed by expanding gasses entrapped under the surface of the casting. For the current study, based on the observed locations of gas entrapment that may induce blistering defects, a surface layer with a thickness of one sixth of the hydraulic diameter of the filling channel ($D/6$) is defined (see Fig. 3a). The entrapped gasses can originate from burned die lubricant or from air entrapped during the die filling process and are compressed during pressure intensification. When the casting is later soaked at a high temperature during solution heat treatment, the pressurized gas pockets expand and deform the surface of the casting to form blisters.

Heating or cooling of the casting will change the pressure inside the trapped gas pocket, and the following equation can be used to predict the influence of a change in temperature upon the gas pressure:

$$\frac{P_1 V_1}{T_1} = \frac{P_2 V_2}{T_2} \tag{1}$$

where $V$ is the volume of the entrapped gas, $T$ is the absolute temperature, $P$ is the pressure inside the gas pocket, and the subscripts represent different states. Fig. 3 illustrates the detailed mechanism of blistering in terms of three separate stages:

*Stage 1*: Gas entrapment occurs during die filling if the cavity filling process is not adequately controlled (*i.e.* the flow front is predominantly planar and laminar but with some instability at the semi-solid/gas interface as in Fig. 1c). As illustrated in Fig. 3a, it is possible for the air to be entrapped into the surface layer and then form a gas $B$ (marked in Fig. 3b). The volume of the entrapped gas $B$ is $V_1$ and the pressure inside the pocket is $P_1$ at this stage.

*Stage 2*: After the cavity is completely filled, the intensification

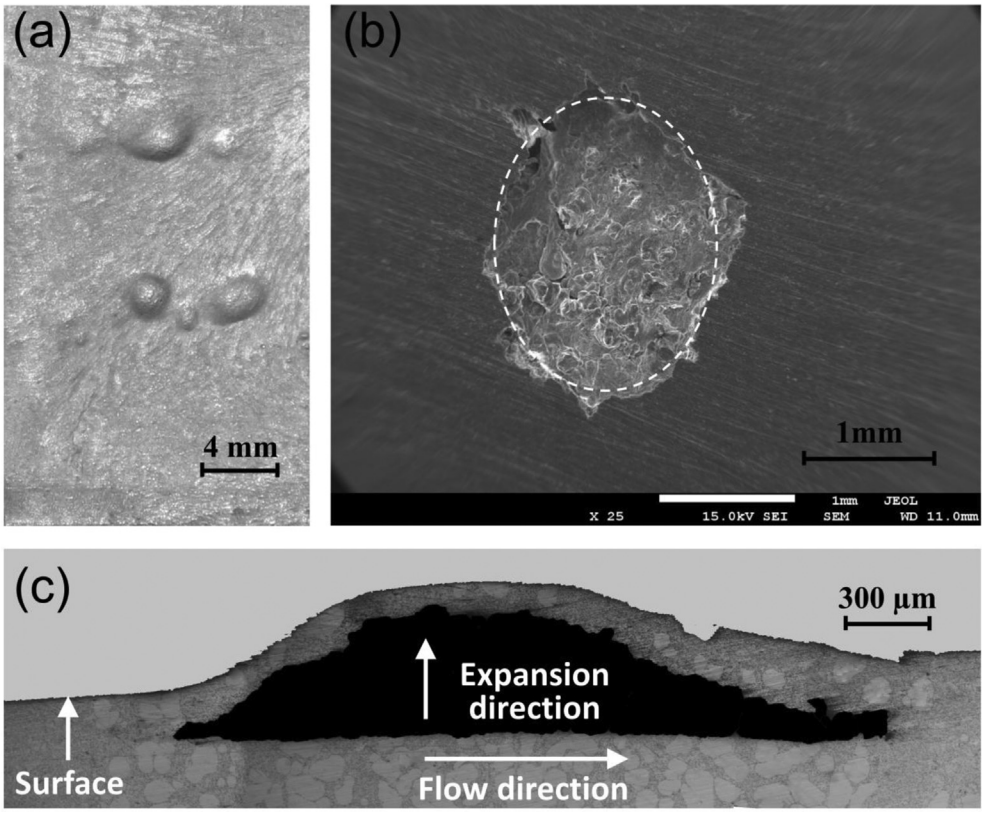


**Fig. 2.** Typical morphology of (a) surface blisters, (b) view of the interior of a gas pocket with the blister cap removed and (c) side view of a gas pocket in a 319 s alloy semi-solid casting.

pressure $P_2$ is applied to the solidifying metal to feed solidification shrinkage. As the runner and gating structure is a closed system, the intensification pressure $P_2$ is transferred to every location within the slurry. According to Eq. (1), therefore, the inside pressure of entrapped gas $B$ will rapidly increase from $P_1$ to $P_2$ as the volume decreases from $V_1$ to $V_2$. However, blistering does not occur at this stage, as the surface of the casting is supported by the mould wall (*i.e.* $F_{mould}$ in Fig. 3b).

*Stage 3*: As the casting solidifies and cools down to room temperature, the volume of the entrapment $B$ stays constant, if the minor contraction as the casting cools is ignored, while the pressure $P_2$ decreases dramatically to $P_2'$. When the casting is then reheated to a temperature $T_3$ during solution heat treatment (about 10–20 K below the solidus temperature of the alloy), the pressure will rise from $P_2'$ to $P_3$. Ignoring the pressure from air which is significantly lower than $P_3$, the blister forms only when the force from the inside pressure $P_3$ exceeds the critical resistance force of the alloy, $F_{alloy}$. The value of $F_{alloy}$, of course, is not constant, but will decrease with increasing temperature as the alloy has lower strength at higher temperatures, and with decreasing depth of the entrapment location below the casting's surface. The blister will eventually stop growing when the force from the decreased pressure $P_3'$ (see Fig. 3c) is equal to $F_{alloy}$.

### 2.2. Mechanics of blistering

It should be noted that the presence of entrapped gas may not always result in the formation of a blister, as illustrated by entrapment $A$ in Fig. 3. According to the mechanism of blistering presented here, there are several critical factors that control whether or not a blister will form, including the initial dimensions and location of the gas pocket, the magnitude of the intensification pressure, and the heat treatment temperature. To demonstrate the relationship between the possibility of blistering and the factors described above, a simple calculation can be performed to analyse the stress distribution in a layer between the blister and the surface of the casting under uniform pressure. As the entrapped gas has been compressed under high pressure intensification, it will be treated as an ellipsoid, having a much shorter radius in the $y$ direction compared with dimensions in the other two directions (*i.e.* $a \geq c \gg b$ in Fig. 4). As a result, the surface layer above the entrapped gas can be approximately assumed to be a flat plate in the $xz$ plane. Under a uniformly distributed pressure $p$ over the entire surface, the stresses on the constant thickness plate with fixed boundary are solved using different theories depending on the plate thickness.

When the plate thickness $t \leq c/4$, the Kirchhoff–Love theory for thin plates [9] is adopted. The stress concentrations at the edge of the plate are then [10]:

$$\text{at the edge of span c}: \sigma_{max} = \sigma_z = \frac{6pc^2}{t^2\left(3 + 2\alpha^2 + 3\alpha^4\right)} \tag{2}$$

$$\text{at the edge of span a}: \sigma_x = \frac{6pc^2\alpha^2}{t^2\left(3 + 2\alpha^2 + 3\alpha^4\right)} \tag{3}$$

where $\sigma$ is the stress, and the subscripts represent different directions, $p$ is the loading pressure, and $\alpha$ equals $c/a$ ($0 < \alpha \leq 1$). The maximum deflection occurs at the centre of the plate:

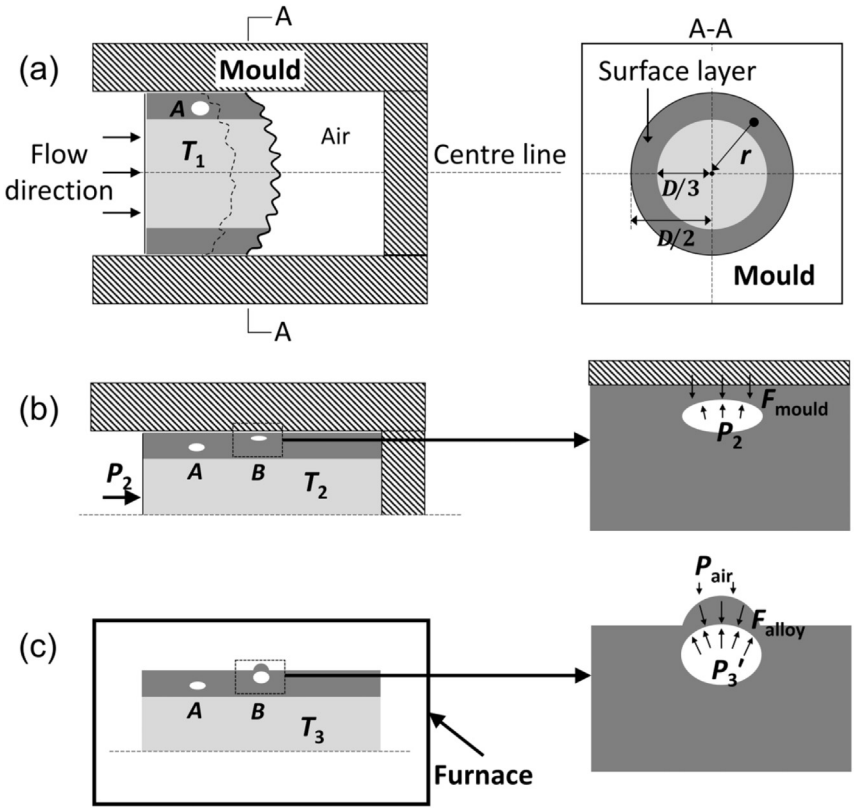


**Fig. 3.** Schematic drawing illustrating the mechanism of surface blistering based on the form of semi-solid flow shown in Fig. 1c with some instability (a) Semi-solid die filling process, (b) Pressure intensification during casting and (c) Solution heat treatment at $T_3$.

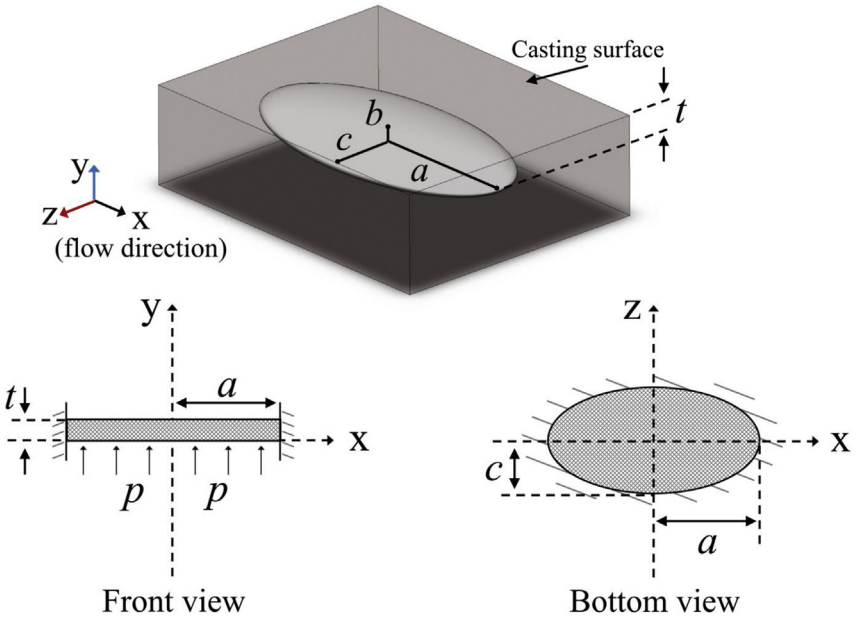


**Fig. 4.** Schematic drawing simplifying the pressured surface layer as a flat plate with fixed boundary.

$$y_{max} = \frac{3pc^4(1-\mu^2)}{2Et^3(3+2\alpha^2+3\alpha^4)} \quad (4)$$

where $\mu$ and $E$ are the Poisson's ratio and Young's modulus of the material, respectively.

From formula (2), the thicker the plate, the higher the pressure that is needed for plastic deformation. Also, $\sigma_{max}$ decreases with increasing $\alpha$ and reaches its minimum when $\alpha$ equals 1, indicating a circular plate. Combining Eq. (1) and Eq. (2), the variation in $\sigma_{max}$ with heat treatment temperature $T_2$ is given by:

$$\sigma_{max} = \frac{6c^2}{t^2(3+2\alpha^2+3\alpha^4)} \cdot \frac{V_1 P_1}{V_2 T_1} \cdot T_2 \quad (5)$$

where the subscript 1 repensents the state before heat treatment, and subscript 2 repensents the state during heat treatment. At a given material thickness $t$, and pocket dimensions $a$ and $c$, Eq. (5) shows that $\sigma_{max}$ linearly increases with increasing heat treatment temperature before any deformation occurs (*i.e.* $V_1 = V_2$). The plate will be plastically deformed and form the surface blister once the stress exceeds the yield strength of the material at the critical temperature indicated in Fig. 5. Once the plastic deformation occurs, $\sigma_{max}$ changes non-linearly as the gas volume increases (*i.e.* $V_2 > V_1$).

When $t \geq c/4$, the plate in Fig. 4 can be analysed by Mindlin–Reissner theory for thick plates [11], where shear deformations are considered, and rotation and lateral deflections are decoupled. Due to the various governing equations for the thick plate model, this classical problem is always solved by means of FEM modelling. For the thick plate, Toda et al. [1] and Maslovskaja et al. [12] have analysed the problem in detail and this will not be discussed further in this paper.

The industrial alloy 319s (Al-5.8%Si-3.0%Cu-0.36%Mg-0.2%Ti, all refer to wt%) will be used here as an exemplar. This alloy was specially developed from the low-cost foundry alloy 319 to have improved semi-solid formability and mechanical properties [6,13]. The semi-solid slurry of 319s is typically produced at 853 K for the die filling process. The temperature of the surface layer is about 850 K [14] before an intensification pressure of 100 MPa is applied to the casting. During subsequent solution heat treatment, the casting is held at 773 K for about 6 hrs. Based on the combined gas law shown in Eq. (1), if no plastic deformation occurs, the gas pressure $P_3$ at the solution heat treatment temperature will be about 91 MPa. The likelihood of blistering occurring will then be determined by the depth and dimensions of the entrapped gas pocket. According to Eq. (2), the maximum stress is equal or greater than $12P_3$ (1092 MPa) if the depth of the gas pocket from the surface is less than one-quarter of the minimum transverse dimension, which is much higher than the yield strength of 319s alloy (350 MPa at room temperature [15]). Therefore, blistering will occur under this condition.

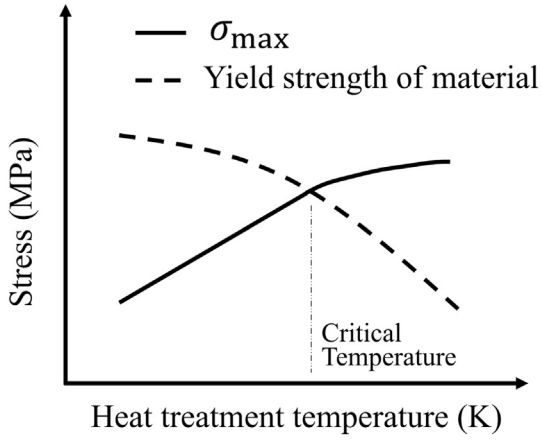


**Fig. 5.** Schematic diagram showing yeild strength of the alloy decreasing with temperature and the relationship between $\sigma_{max}$ in Eq. (2) and the heat treatment temperature ($T_2$). Below the cross-over point the relationship is linear and above it non-linear.

## 3. Factors affecting gas entrapment in the surface layer

Although there are several factors which influence blistering, the most effective approach for avoiding blistering is to minimize the entrapment of gasses during the die filling process, rather than controlling the pressure intensification or heat treatment. Therefore, it is important to understand how the process parameters affect the entrapment during the filling process. Here the flow behaviour of the surface layer will be characterized to examine the stability of flow at different process conditions. The most commonly-applied dimensionless number to determine the internal flow state, especially in runner and gating systems, is the Reynolds number *Re* [16]:

$$Re = \frac{\rho D^n v^{2-n}}{\eta} \quad (6)$$

where $\rho$ is the density of alloy, $D$ is the hydraulic diameter of the conduit, $v$ is the flow velocity, $n$ is an exponent determined by rheological properties of flow and $\eta$ is the viscosity. According to studies on the rheology of semi-solid alloys [17,18], the solid-liquid slurry is typically a shear-thinning fluid and the viscosity $\eta$ can be represented by a power law of the form [18]:

$$\eta = k\dot{\gamma}^{n-1} \quad (7)$$

where $k$ is the consistency factor, $n$ is the flow exponent as in Eq. (6), and $\dot{\gamma}$ is shear rate. (Note that this equation is in some cases a simplification). For normal shear-thinning fluids, the value of $n$ is between zero and unity. However, in previous studies measuring $n$ in semi-solid alloy systems *e.g.* Refs. [19–21], both positive and negative values of $n$ have been obtained. Negative values for $n$ are considered to be related to anomalous rheological behaviour of semi-solid alloys that has not been reported in any other fluid system. McLelland et al. [22] suggested that the negative value of $n$ may be a feature of the rapid breakdown of the internal structure of solid particle clusters which occurs at low shear rates. Eq. (7) only applies in a certain temperature range in which the viscosity change follows a power-law relationship due to structural dis-agglomeration under shear stress. When the temperature, *i.e.* the equivalent liquid fraction, is greater than the upper limit of this range, the flow behaves as a Newtonian liquid even in the semi-solid state because no dis-agglomeration of particle clusters occurs at low solid fractions.

Assuming a fully developed laminar flow in a circular conduit, the shear rate is given by Ref. [16]:

$$\dot{\gamma} = \frac{3n+1}{4n} \times \frac{8v}{D} \left(\frac{2r}{D}\right)^{\frac{1}{n}} \quad (8)$$

where $r$ is the radial distance from the centreline of the conduit (see Fig. 3a), and the hydraulic diameter $D$ is equal to the diameter for pipe flow. The average shear rate of the surface layer, $\bar{\dot{\gamma}}_{surf}$, obtained by integrating throughout the annular cross-section from $r = D/3$ to $r = D/2$, is given by:

$$\bar{\dot{\gamma}}_{surf} = \frac{1}{\pi\left(\frac{D}{2}\right)^2 - \pi\left(\frac{D}{3}\right)^2} \int_{\frac{D}{3}}^{\frac{D}{2}} \dot{\gamma} \cdot 2\pi r dr = \frac{(108n+36)v}{(10n+5)D}\left(1 - \left(\frac{2}{3}\right)^{\frac{1+2n}{n}}\right) \quad (9)$$

Combining Eqs. (6), (7) and (9) leads to

$$Re_{surf} = \frac{\rho D^n v^{2-n}}{k\left[\frac{(108n+36)v}{(10n+5)D}\left(1-\left(\frac{2}{3}\right)^{\frac{1+2n}{n}}\right)\right]^{n-1}} \quad (10)$$

where $Re_{surf}$ is the average Reynolds number of the defined surface layer ($D/6$). As can be seen in Eq. (10), the average Reynolds number of the surface layer is related to the flow velocity, the dimensions of the cavity and the temperature-dependent rheological parameters.

Isothermal semi-solid compression tests were carried out to investigate rheological properties of the 319s alloy according to the methodology in Refs. [21,23]. All the tests were conducted using a high frequency fatigue tester (MTS Landmark 370) equipped with a model 653 high-temperature furnace. This machine provides high-speed closed-loop control and data acquisition. The samples ($\Phi 12 \times 12$ mm) were heated from room temperature to a temperature of 843 K, 848 K or 853 K in about 8 min and then compressed immediately at a constant ram speed of 0.1 m/s. Fig. 6 shows the evolved microstructures before rapid compression. All the samples for microstructural examination were water-quenched after being heated to the desired temperatures. Fig. 6d shows the liquid fraction at different temperatures, and the liquid fraction of a slug for practical thixocasting heated to 853K by induction heating is also presented for comparison. This shows that the remelting route in this experiment is close to practical thixocasting and therefore practical casting can be used to verify the theory based on compression test data. Note that the liquid fraction here is the effective liquid around α-aluminium particles excluding any liquid entrapped in the body of the α-aluminium particle.

Assuming a Newtonian fluid and a constant volume of specimen during compression, the apparent viscosities and corresponding shear rates were calculated from the measured load-displacement curves (Fig. 7a) at different temperatures by applying the following analytical formulae [23], with the compression carried out at a constant ram speed.

$$\eta = \frac{2F\pi H^5}{3\nabla^2 v_{ram}} \quad (11)$$

$$\dot{\bar{\gamma}} = \frac{R}{2H^2}\cdot v_{ram} \quad (12)$$

where $H$ and $R$ are the instantaneous height and radius of the specimen respectively, $\nabla$ is the volume of the specimen, $F$ is the measured force and $v_{ram}$ is the constant ram speed. Fig. 7b shows the calculated viscosities have a linear relationship with shear rate on a log-log scale. On the basis of the power law viscosity model in Eq. (7), the values of the flow parameters *n-1* and *k* were derived by linear fitting analysis. As discussed above, the value of *n-1* approaches zero with decreasing solid fraction to lower than a critical value. In the previous work by Figueredo et al. [24], the semi-solid slurry (A357 alloy) was observed to behave as a Newtonian fluid ($n = 1$) once the liquid fraction reached about 0.85. Fig. 8 shows that the parameters obtained in this study (and that from Figueredo et al. [24]) further fitted as functions of the absolute temperature following the sigmoidal function in software package Origin 2015 (Non-commercial version).

Employing Eq. (10) and considering industrial semi-solid casting practices, the average Reynolds numbers at the defined surface layer (assumed to be $D/6$ thick) were determined and plotted in

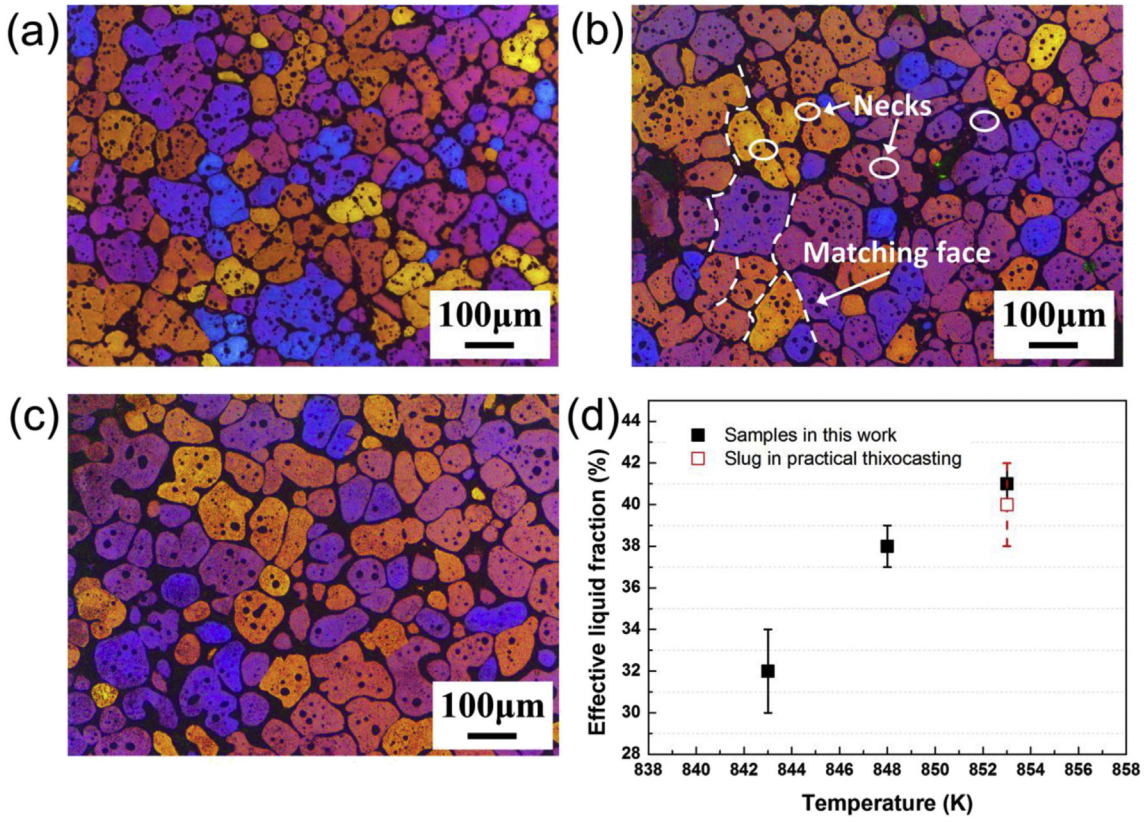


**Fig. 6.** Evolved microstructures (once the set temperature is achieved) in rapid compression samples heated to different temperatures. (a) 843 K, (b) 848 K, (c) 853 K, (d) effective liquid fraction including that for a slug heated to 853 K in practical process.

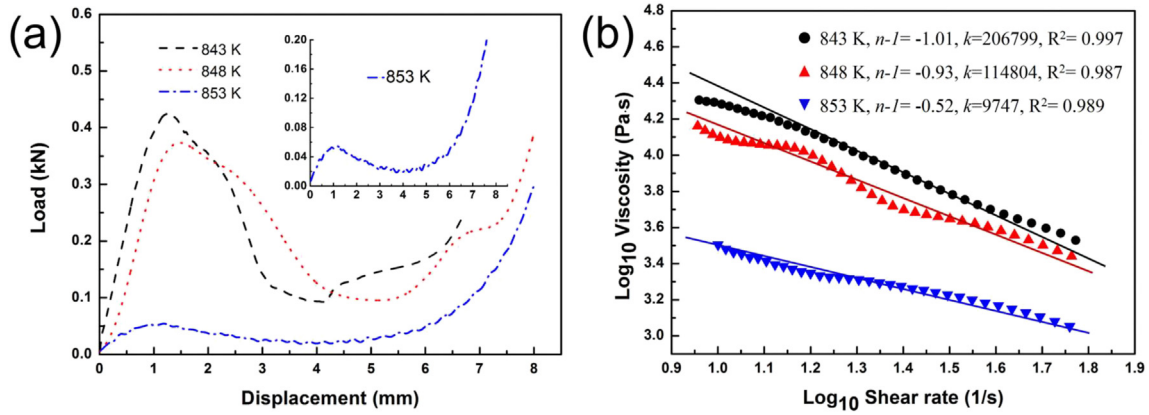


**Fig. 7.** Determination of the flow parameters in power law model for semi-solid 319s alloy. (a) The load-displacement signals at different temperatures, (b) calculated viscosities versus shear rate based on the Laxmanan and Flemings methodology [23].

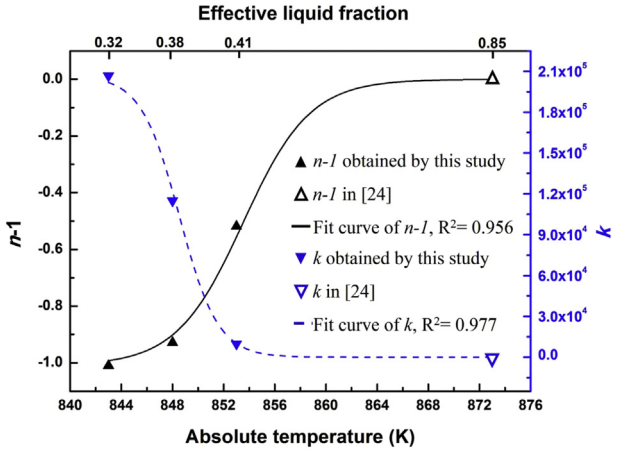


**Fig. 8.** Fitted curves for temperature-dependent flow parameters of 319s alloy.

Fig. 9. Fig. 9a and b illustrate that the Reynolds number increases with an increase in the flow velocity, whereas there are differing correlations with increasing hydraulic diameter. When the temperature is lower than 853K (marked in Fig. 9d), the Reynolds number decreases with increase of hydraulic diameter. However, the Reynolds number increases with increase of diameter if the temperature is higher than 853K. Fig. 9c shows the calculated *Re* based on the temperature-dependent flow parameters shown in Fig. 8 and on the basis of predicted Newtonian viscosities. The curves shown in Fig. 9c lead to the *counter-intuitive* result that *Re* initially decreases with increase of temperature, followed by a rise, indicating a minimum value at about 858 K, and is then relatively constant once the temperature is greater than the liquidus temperature. In general, higher *Re* indicates more unsteady flow during the die filling process and hence a greater probability of the entrapment of the lubricant or air into the surface layer of the casting. Thus, there is a critical value of *Re* below which the flow is steady enough to avoid gas entrapment. As illustrated in Fig. 9c, the temperature window from $T_3$ to $T_4$ is the optimal filling process window in which the filling can be best controlled to minimize entrapment. However, practical experience with semi-solid casting suggests the window for slurry preparation is $0.3 < f_l < 0.5$ [25], *e.g.* for 319s alloy, the slurry is normally prepared at a temperature range from $T_1$ to $T_2$, where $0.3 < f_l < 0.5$, to ensure a suitable slurry consistency. Therefore, as indicated in Fig. 9c, there must be a process window (from $T_3$ to $T_2$) for semi-solid die casting for both optimum solid fraction *and* controlled filling process. It can be seen from Fig. 9d that increasing the value of *v/D*, *i.e.* increasing the shear rate according to Eq. (8), will increase the sensitivity of Reynolds number to temperature. At a constant filling velocity and a certain critical *Re*, enlarging the sectional diameter of the casting (*i.e.* a lower value of *v/D)* will increase the process window, implying that castings with thicker walls are less likely to entrap gas. Note that, as shown in Fig. 9a, the highest Reynolds number in the temperature window of interest is less than 2300, which is generally considered as the critical value for the flow state transition from laminar to mixed flow [26]. A relatively high Reynolds number also indicates greater instability even when the flow remains essentially laminar. As a result, the air or die lubricant near the wall will be more easily entrapped inside the surface layer the higher the *Re* of the surface layer. It is concluded that increasing the flow velocity and decreasing the flow diameter will increase the probability of entrapment of gas and hence of the surface blistering.

Fig. 10 shows a schematic drawing of the semi-solid flow state in terms of the spheroidal particles as the liquid fraction increasing. For a relatively low fraction liquid from ~0.3 to ~0.4, as shown in Fig. 10a, the particles are quite closely packed and tend to collide and rotate (marked by bidirectional arrows) The liquid flows from high static pressure zone to lower one (marked by dotted arrows), leading to a relatively unsteady interfacial flow state. At medium liquid fraction from ~0.4 to ~0.5 (Fig. 10b), the liquid fills the channels between the particles uniformly and the two phases interact synergistically, resulting in a steady flow state. As the liquid fraction continues to increase (>0.5), the liquid phase begins to dominate the flow behaviour, as indicated by solid arrows in Fig. 10c and the interface between the semi-solid flow front and the gas will start to exhibit some instability. This provides a rationale for the counter-intuitive nature of Fig. 9c with the curve of Reynolds number versus temperature initially *decreasing* and then increasing.

## 4. Experimental validation of the theory

Practical thixocasting was carried out to verify the effects of process parameters on surface blistering. Fig. 11 shows an illustration of the injection and gating systems. Here the castings for blister examination were produced using a step die, containing five separate sections of different thickness. A 340-ton Buhler horizontal cold chamber die casting machine with a large-diameter shot cylinder specially modified for semi-solid casting was utilized. Slugs 89 mm in diameter and 178 mm tall were cut from the

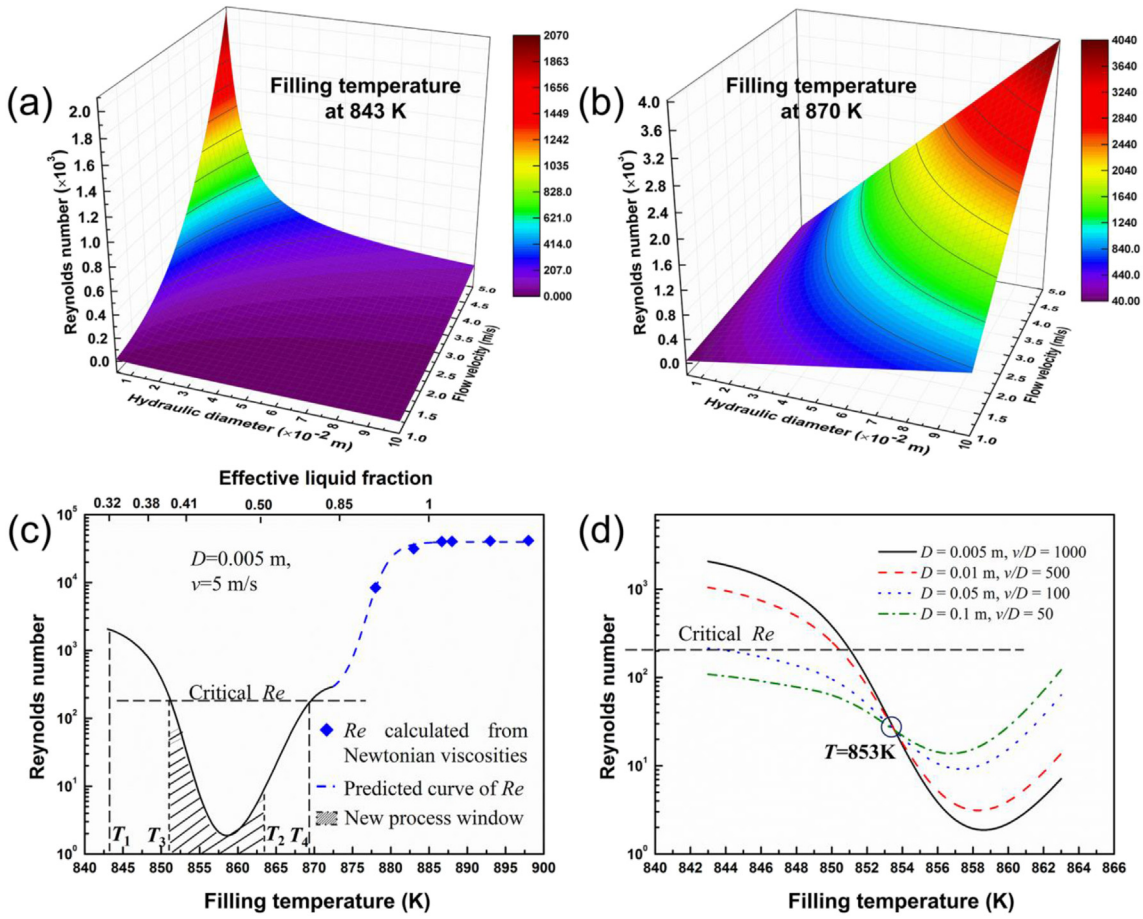


**Fig. 9.** Average Reynolds number of the $D/6$ thick surface layer, indicating the effects of filling parameters on the flow stability ($\rho_{319s}$ = 2600 kg/m$^3$) of the 319s alloy at (a) Temperature 843 K and (b) Temperature 870 K, (c) *Re* curve as a function of filling temperature for $D$ = 0.005m, $v$ = 5 m/s and (d) for different $v/D$ values.

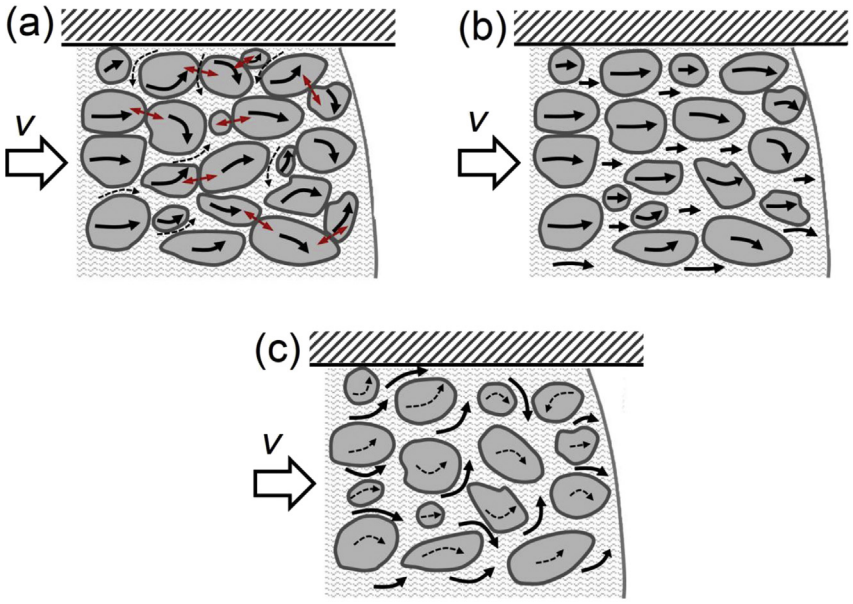


**Fig. 10.** Schematic diagram of semi-solid interior flow state as liquid fractions increasing. (a) relatively low liquid fraction (~0.3–~0.4), (b) medium liquid fraction (~0.4–~0.5) and (c) relatively high liquid fraction (>0.5).

pre-cast semi-solid feed material and reheated to 853K and 863K using a 10-coil carousel-style induction heater. The die was heated and held at about 523 K. Different intensification pressures and filling velocities were also adopted. After production of

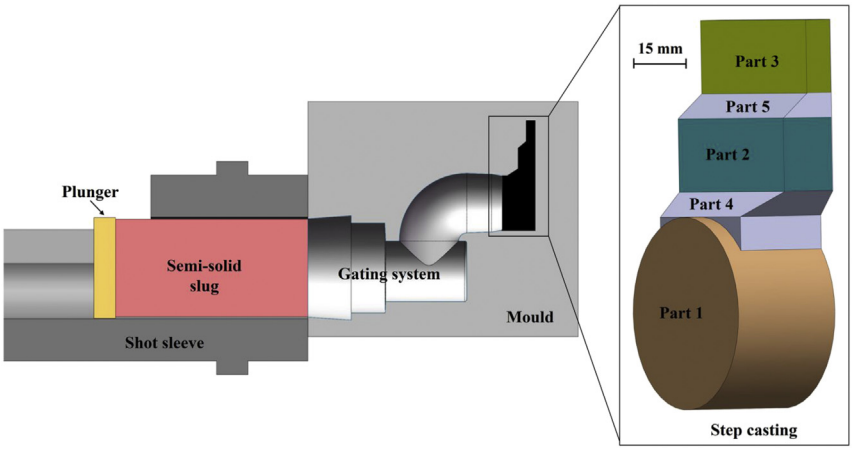


**Fig. 11.** Illustration of the injection system and gating system of semi-solid die casting using a step die.

**Table 1**
Scoring method used for characterizing the size of blisters.

| Maximum blister size (mm) | <0.1 | 0.1–0.5 | 0.5–1.0 | >1.0 |
|---|---|---|---|---|
| Blister score | 0 | 1 | 2 | 3 |

components with the various process parameters, the castings were solution treated at 773 K for 2 hrs and then water quenched. As shown in Fig. 2, blisters of different sizes were generated during solution treatment. To quantify the level of blistering, the size of the largest blister in each of the five separate parts (*i.e. Part* 1 to *Part* 5) was measured and scored using the method presented in Table 1. The five scores for each casting were averaged, providing an overall score for each processing condition. In addition, as there was some variation in the level of observed blistering even for a series of castings produced under the same conditions, the results discussed in this study are the average values for at least 8 castings produced under the same process parameters.

The average blistering scores for castings produced under the various process conditions are listed in Table 2. Note that the results obtained in simulations show that the actual temperatures of the semi-solid slurry when filling the cavity are about 3–6 K lower than the slug temperatures recorded in Table 2, arising from heat loss to the runner and gating system during filling the die. The data in Table 2 show that increasing intensification pressure and flow velocity lead to an increase in the level of blistering in the semi-solid die castings. Most importantly for the analysis presented in *Section* 3 of this paper, the data in Table 2 confirm that a lower level of blistering was also observed with a higher slurry temperature. This disagrees with conventional wisdom, which suggests that a lower temperature slurry should have less entrapped gas, due to the higher viscosity of the slurry. However, these results agree well with the analysis presented in *Section* 3, which suggests that the Reynolds number of the slurry is actually lower at 863 K than that at 853 K, and it would expected that more gas would be entrapped at the lower temperature.

The blistering scores of actual industrial parts with different thickness (parts 1–3 shown in Fig. 11) have been further examined and the results are given in Table 3. It can be seen that the blistering scores increase with increase of the values of $v/D$, *i.e.* decrease of the part thickness, for slugs prepared at 853 K. However, no significant difference in the blistering scores was observed when the slug temperature was 863 K. According to Fig. 9d, increasing values of $v/D$ promotes the instability of the slurry and hence a still higher blistering score is expected when the filling temperature is less than 853 K. Assuming the slurry filling temperature is about 860 K

**Table 2**
Blistering level of semi-solid die castings produced using 319s alloy under different process conditions.

| Process conditions | | | Average score |
|---|---|---|---|
| Intensification $P$ (MPa) | Plunger velocity (m/s) | Slug temperature (K) | |
| 112 | 0.12 | 863 | 0.30 |
| | | 853 | 0.67 |
| | 0.25 | 863 | 0.28 |
| | | 853 | 0.83 |
| | 0.50 | 863 | 0.36 |
| | | 853 | 1.14 |
| 90 | | | 1.13 |
| 41 | | | 0.20 |

**Table 3**
Blistering level of the parts with different thickness, indicating the impact of thickness on blistering. The table shows the data for two different slug temperatures.

| Parts | Plunger velocity (m/s) | Filling velocity/Hydraulic diameter ($v/D$) | Average score ($T_{slug}$ = 853 K) | Average score ($T_{slug}$ = 863 K) |
|---|---|---|---|---|
| Part 1 | 0.25 | 18 | 0.6 | 0 |
| Part 2 | | 102 | 1.1 | 0.2 |
| Part 3 | | 362 | 1.9 | 0 |

for a slug temperature of 863 K, Fig. 9d suggests that the Reynolds numbers are much lower than the critical *Re* for blistering resulting in acceptable blistering levels in spite of the different part thickness.

## 5. Summary and conclusions

Blister formation is associated with the entrapment of gas whether from air in the die or from burned lubricant. In semi-solid casting the flow in the die is essentially laminar (in contrast with high pressure die casting). Here firstly the mechanics of formation of the blister has been presented (with the gas pressure in the entrapped pocket rising during heat treatment to a point where the yield stress of the overlying cap of material is exceeded and the blister forms). The Reynolds number in the surface layer of the flow is then analysed to obtain the relationships with hydraulic diameter and flow velocity for different slurry temperatures (and hence fraction liquid). The hypothesis is that it is some flow instability at the flow front, even where the overall nature of the flow is essentially laminar, which is leading to the entrapment of the gas. This is occurring primarily at the layer which is in contact with the die but may occur elsewhere. The crucial finding is that if the Reynolds number is plotted against temperature there is a decrease followed by an increase (Fig. 9c). The position of this minimum is dependent on the ratio of fill velocity to the hydraulic diameter *v/D* (Fig. 9d). Thus there is a 'sweet spot' in terms of temperature (*i.e* fraction liquid) where the flow front has the maximum stability (hence giving maximum resistance to blister formation). This is in contrast with conventional wisdom which would suggest that low fractions liquid (within the processing range of 0.3 fraction liquid to 0.5 fraction liquid) would give the most stable flow front. A rationale for this is presented in terms of the particle crowding at the relatively low fraction of liquid.

Experimental results for blistering with aluminium alloy 319s as an exemplar and a die which has varying cross sectional dimensions (and hence hydraulic diameters *D*) are presented and validate the hypothesis.

## Acknowledgements

Financial support from the National Key Research and Development Program of China (No.2016YFB0301001) is gratefully acknowledged. The authors would like to thank Dr. Daquan Li and Dr. Hongxing Lu for helpful discussions. Mr. X.G.Hu also thanks Chinese Scholarship Council (CSC) for financial support and the University of Leicester for hosting his visiting research.

## References

[1] H. Toda, P. Qu, S. Ito, K. Shimizu, K. Uesugi, A. Takeuchi, Y. Suzuki, M. Kobayashi, Formation behaviour of blister in cast aluminium alloy, Int. J. Cast. Metal. Res. 27 (2014) 369–377.
[2] E.J. Vinarcik, High integrity die casting processes, John Wiley & Sons, 2002.
[3] I. Gattelli, G. Chiarmetta, M. Boschini, R. Moschini, M. Rosso, I. Peter, New generation of brake calipers to improve competitiveness and energy saving in very high performance cars, Solid State Phenom. 217 (2015) 471–480.
[4] D.H. Kirkwood, Semisolid metal processing, Int. Mater. Rev. 39 (1994) 173–189.
[5] S. Janudom, J. Wannasin, J. Basem, S. Wisutmethangoon, Characterization of flow behavior of semi-solid slurries containing low solid fractions in high-pressure die casting, Acta Mater. 61 (2013) 6267–6275.
[6] S.P. Midson, Industrial applications for aluminum semi-solid castings, Solid State Phenom. 217 (2014) 487–495.
[7] North American Die Casting Association, NADCA product specification standards for die castings produced by the semi-solid and squeeze casting processes, 2009. Wheeling, Illinois, USA.
[8] D. Liu, H.V. Atkinson, P. Kapranos, W. Jirattiticharoean, H. Jones, Microstructural evolution and tensile mechanical properties of thixoformed high performance aluminium alloys, Mater. Sci. Eng. A 361 (2003) 213–224.
[9] J.N. Reddy, Theory and Analysis of Elastic Plates and Shells, CRC press, 2006.
[10] W.C. Young, R.G. Budynas, Roark's Formulas for Stress and Strain, McGraw-Hill, New York, 2002.
[11] R.D. Mindlin, Influence of rotatory inertia and shear on flexural motions of isotropic elastic plates, J. Appl. Mech. 18 (1951) 31–38.
[12] O. Ozhoga-Maslovskaja, E. Gariboldi, J.N. Lemke, Conditions for blister formation during thermal cycles of Al–Si–Cu–Fe alloys for high pressure die-casting, Mater. Des. 92 (2016) 151–159.
[13] X.G. Hu, Q. Zhu, H.X. Lu, F. Zhang, D.Q. Li, S.P. Midson, Microstructural evolution and thixoformability of semi-solid aluminum 319s alloy during re-melting, J. Alloys Compd. 649 (2015) 204–210.
[14] X.G. Hu, F. Zhang, Y.F. He, S.P. Midson, Q. Zhu, Experimental study and numerical simulation on the blistering defect during thixocasting, Solid State Phenom. 217 (2015) 144–150.
[15] S.P. Midson, Y.F. He, X.G. Hu, D.Q. Li, F. Zhang, Q. Zhu, Impact of section thickness on the microstructure and mechanical properties of semi-solid castings, in: Shape Casting: 5th International Symposium 2014, John Wiley & Sons, Inc, 2013, pp. 177–184.
[16] J. Hartnett, Y. Cho, in: W. Rohsenow, J. Hartnett, Y. Cho (Eds.), Non-Newtonian Fluids, Handbook of Heat Transfer, third ed., McGraw-Hill, New York, 1998, 10.11-10.53.
[17] H.V. Atkinson, Modelling the semisolid processing of metallic alloys, Prog. Mater. Sci. 50 (2005) 341–412.
[18] H.V. Atkinson (Ed.), Modelling of Semi-solid Processing, Shaker, Aachen, 2008.
[19] C. Quaak: Ph.D. Thesis, Technische Univesiteit Delft, Delft, The Netherlands, 1996.
[20] J. Yurko, M.C. Flemings, Rheology and microstructure of semi-solid aluminum alloys compressed in the drop-forge viscometer, Metall. Mater. Trans. A 33 (2002) 2737–2746.
[21] T.Y. Liu, H.V. Atkinson, P. Kapranos, D.H. Kirkwood, S. Hogg, Rapid compression of aluminum alloys and its relationship to thixoformability, Metall. Mater. Trans. A 34 (2003) 1545–1554.
[22] A.R.A. McLelland, N.G. Henderson, H.V. Atkinson, D.H. Kirkwood, Anomalous rheological behaviour of semi-solid alloy slurries at low shear rates, Mater. Sci. Eng. A 232 (1997) 110–118.
[23] V. Laxmanan, M.C. Flemings, Deformation of semi-solid Sn-15 pct Pb alloy, Metall. Trans. A 11 (1980) 1927–1937.
[24] A. de Figueredo, A. Kato, M.C. Flemings, Viscosity of semi-solid a357 alloy in the transient high shear rate regime, Metall. Sci. Technol. 18 (2013) 32–36.
[25] D. Liu, H.V. Atkinson, H. Jones, Thermodynamic prediction of thixoformability in alloys based on the Al–Si–Cu and Al–Si–Cu–Mg systems, Acta Mater. 53 (2005) 3807–3819.
[26] J. Holman, Heat Transfer, 9th, McGraw-Hill, 2002.